





2002-08

# On Control of Autonomous Circular Parachute

Yakimenko, O.

Yakimenko, O., Dobrokhodov, V., Johnson, J., Kaminer, I., Dellicker, S., and Benney, R., "On Control of Autonomous Circular Parachute," Proceedings of the AIAA Guidance, Navigation, and Control Conference, Monterey, CA, August 5-8, 2002.
http://hdl.handle.net/10945/50419

AIAA Guidance, Navigation, and Control Conference and Exhibit
5-8 August 2002, Monterey, California

AIAA 2002-4753
AIAA 2002-4753

# ON CONTROL OF AUTONOMOUS CIRCULAR PARACHUTES

**O.Yakimenko, V.Dobrokhodov, J.Johnson, I.Kaminer**
*Naval Postgraduate School, Monterey, CA*
**S.Dellicker**
*U.S. Army Yuma Proving Ground, Yuma, AZ*
**R.Benney**
*U.S. Army Soldier and Biological Chemical Command, Natick, MA*



This paper addresses the development of autonomous guidance, navigation and control algorithms for a flat solid circular parachute. This effort is a part of the Affordable Guided Airdrop System (AGAS) that integrates a low-cost guidance and control system into fielded cargo air delivery systems. First the paper describes underlying AGAS concept, architecture and components. Then it suggests a synthesis of a classical optimal control for the AGAS based on Pontrjagin's maximum principle. It also gives an explanation of the practical control algorithm implemented in simulations and in flight tests of AGAS and provides some key examples. Results of the final AGAS demonstration performed at the U.S. Army Yuma Proving Ground in September 2001 are also presented. The paper ends with conclusions.

## I. Introduction

As identified in Ref.1 there is an urgent need to improve the point-of-use delivery; that is, getting the materiel where it needs to be and when it needs to be there. This statement served as an initial point for the AGAS project, initiated by the U.S. Army and by the U.S. Air Force in late 90s.[2,3]

Currently, high-altitude/low-opening and high-altitude/high-opening airdropped personnel are the only assets that can be released from altitudes above 1500*m* while still realizing an acceptable landing accuracy. Aerial missions over Bosnia in 1993 underscored high-altitude airdropped payload delivery accuracy concerns during operations conducted from above 3000*m* for resupply and humanitarian purposes (a lot of cargo ended up at the wrong spots). Humanitarian-relief airdrops over Kosovo in 1999 and Afganistan in 2001 demanded that airdrop aircraft operate from even higher altitudes, with an expected further degradation of payload delivery accuracy.

These facts have led to the main design goal of the AGAS development - to provide guidance, navigation, and control (GNC) system that can be placed in-line with existing fielded cargo parachute system (G-12) and standard delivery containers (A-22). The system was required to provide an accuracy of at least 100*m* with a desired goal of 50*m* circular error probable (CEP). No changes to the parachute or cargo system were allowed.

As a first step to address the problem of GNC development for AGAS a reliable parachute model must be available. An extensive literature search was conducted to determine that no fully validated model exists[4-20]. Although the basic equations for the 6-DoF model are known[6], there is still some uncertainty about the definition and computation of the added mass tensor. Aerodynamic force and moment coefficients are poorly defined as well. Finally there is very little data verifying parachute model using flight test data.

Furthermore, while autonomous control of the high-glide parafoils has been studied extensively[21-24], nothing was found on the autonomous control of a low-glide circular parachute. The only results reported beyond uncontrolled dynamics of round parachutes and CFD-based aerodynamics of their canopy addressed open-loop stability[13-20].

Therefore initial investigation of the anticipated performance of the AGAS system used a simple 3-DoF model incorporating sensor and actuator dynamics and a simple bang-bang control strategy. Two major objectives were pursued. First - to verify the effectiveness of the "predefined-trajectory seeking" control strategy with a good wind estimate versus a control strategy that simply seeks the target area (TA) without using any knowledge of the winds. Second - to estimate the impact of changing the characteristics of the sensor suite and actuator dynamics on the overall system performance[25,26]. The resulting GNC algorithm was successfully tested in simulation[27].

Initial flight tests of this GNC algorithm showed the inadequacy of a 3-DoF model. In particular, certain physical phenomenon has been observed that the 3-DoF parachute model could not predict. Therefore, the second stage of research aimed primarily at flight-testing designed algorithms and included the development of a complete 6-DoF model of controlled circular parachute[28]. This stage also included extensive hardware-in-the loop simulation[29,30].

In 2001 about 15 drops were accomplished at the U.S. Army Yuma Proving Ground, Yuma AZ (YPG). These drops have led to a better understanding of the dynamics of the parachute, improve hardware design for the control system, fix and tune GNC algorithms.

This paper reviews the AGAS project starting with the underlying concept, architecture and components of the system (Section II). It continues with the classical synthesis of an optimal control using Pontrjagin's Maximum Principle (Section III), followed by a de-

scription of the flight control algorithm implemented in simulations and flight test (Section IV). Section V describes some key simulations and tradeoffs. Finally Section VI shows the setup and results of a final flight test performed at the YPG in September 2001[31].

## II. System architecture and components

### II.1. AGAS concept

The key ideas of AGAS concept can be easily understood by exploring Fig.1.

The first step is to broadcast a supply request that includes information on where and when it is needed on the ground (Fig.1a). Upon arrival at the assigned drop zone (DZ) the delivery aircraft drops a wind dropsonde (Fig.1b). The wind profile acquired during this drop allows computation of the reference trajectory (RT) and of the Computed Air Release Point (CARP). The aircraft will then be navigated to that point for air delivery of the materiel (payload). Should the wind estimate and calculation of CARP be perfect and the aircrew gets the aircraft to this point precisely, then the parachute would fly along RT towards the TA with no control inputs required (Fig.1c). However, wind estimation is not a precise science. Furthermore, calculation of the CARP relies on less than perfect estimates of the parachute aerodynamics and the flight crews cannot precisely hit CARP for each airdrop mission (especially in case of massive (multiple) deliveries). Therefore, the AGAS GNC system is used to overcome these potential errors.

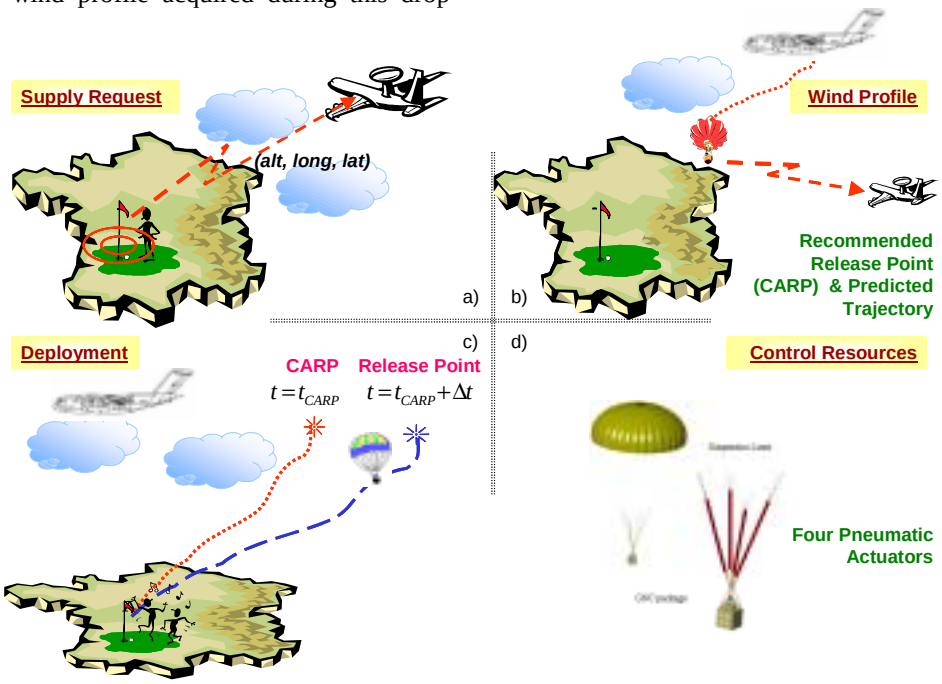


Fig.1 - AGAS concept

The ultimate goal of the AGAS system is to allow delivery aircraft to accurately drop payloads at or above 5500*m*, keeping the aircraft out of the range of shoulder fired ground to air missiles. Another benefit of the system is the ability to pre-address each bundle in a load and to guide the individual bundles to their own pre-programmed TA. Obviously, in order to accomplish these goals, the AGAS system needs to be simple, affordable, durable, and reusable (it should survive multiple drops without any repairs). It should not require major modifications to the standard delivery system's harness or bundle, major modifications to the cargo parachute, or a significant amount of rigger training.

As a result, the AGAS design concept employs commercial Global Positioning System (GPS) receiver and a heading reference as navigation sensors, an inexpensive guidance computer to determine and activate the desired control inputs, and application of Pneumatic Muscle Actuators (PMAs) to generate control inputs. The navigation system and guidance computer are secured to existing container delivery system, while PMAs are attached to each of four parachute risers and to the container (Fig.1d). Control is affected by lengthening one or two adjacent risers. Upon deployment of the system from the aircraft, the guidance computer steers the system along pre-planned RT. The AGAS concept relies on the sufficient control authority to be produced to overcome errors in wind estimation and the point of release of the system from the aircraft. Following subsections briefly discuss main components of the developed and flight-tested G-12 based AGAS.

### II.2. Parachute

In general, AGAS may be implemented on any circular parachute (a flat circular parachute is the one that when laid out on the ground forms a circle). C-9 and G-12 parachutes[23,33] were modeled so far to demonstrate feasibility of the AGAS concept. Although C-9 was initially designed as an ejection seat parachute, it is a standard flat circular parachute as is the larger G-12 cargo parachute on which AGAS will ultimately be used. Some general data on these parachutes can be found in the Tab.1.

Tab.1. Parachute data

| Parameter | C-9 | G-12 |
|---|---|---|
| $d_0$ $(m)$ | 8.5 | 19.5 |
| $d_P / d_0$ | 0.67 | 0.67 |
| Number of suspension lines | 28 | 64 |
| $l_0 / d_0$ | 0.82 | 0.80 |
| $C_{D0}$ | 0.68 | 0.73 |
| Parachute weight (*kg*) | 5.1 | 59 |
| Payload weight (*kg*) | 91 | 998 |
| Descent rate at sea level* (*m/s*) | 6.1 | 8.5 |

In this table $d_0$ denotes the nominal diameter of the parachute, $d_P$ - inflated canopy diameter, $C_{D0}$ - drag coefficient, and $l_0$ - suspension line length.

A cargo box of G-12 parachute that is currently employed for the AGAS is a prototype adopted from A-22 delivery container with the capacity of carrying almost a ton. It is suspended from the system and houses GNC system, PMAs, and instrumentation system. A standard G-12 uses Y-bridle pairs separated into four equal length risers. The parachute is packed into a standard G-12 deployment bag. The PMAs (Fig.2a) are stowed in the riser extension sleeve that is part of the G-12 deployment bag (Fig.2b).

II.3. Actuators and pneumatic control system

To provide control inputs for AGAS, Vertigo, Inc. developed PMAs (Fig.2a) that are braided fiber tubes with neoprene inner sleeves that can be pressurized[35-37]. Upon pressurization, the PMA contracts in length from 7.6*m* to 5.8*m* and expands in diameter. Upon venting it does the opposite (lengthens on 30%).

a)



b)

Fig.2 – Vertigo's PMAs (a); and G-12 parachute and PMAs in deployment bag (b)

When three of four PMAs are pressurized (filled) and one is activated (vented) this action "deforms" the parachute creating an unsymmetrical shape, essentially shifting the center of pressure, and providing a drive or slip condition. This forces the parachute to glide in the opposite direction of the control action (vented PMA). Two adjacent PMAs can be activated simultaneously. Fig.3 shows both possibilities (one and two PMAs activated) realized in CDF-based simulation[34] and observed in the flight test during the air drops at YPG.

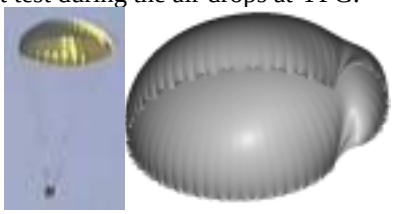

a)

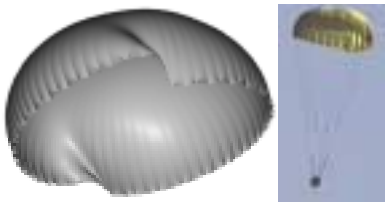

b)

Fig.3 - One (a) and two (b) PMAs actuated (vented)

The volume of the onboard nitrogen tank limits the number of possible fills for all four PMAs to 32 per drop. PMA fill and vent times remain the constant 5…6 seconds throughout each drop (regardless the of the volume of gas remaining in the tanks). Tab.2 characterizes control authority available to the GNC system of the AGAS.

Tab.2. AGAS performance

| Number of PMAs activated | 0 | 1 | 2 |
|---|---|---|---|
| Descent rate $V_z$ at 3000 *m (m/s)* | 8.43 | 8.16 | 7.93 |
| Glide Ratio (GR) | 0 | 0.37 | 0.52 |

The PMAs' control system (PCS) also developed by Vertigo, Inc. resides in a specially designed container of 0.4*m* height (Fig.4a)[37]. It consists of high-pressure recharge circuit (225*atm*), two 44*atm* accumulator tanks, pressure reduction units, valves, low-pressure circuit feeding PMAs (10.2*atm*). Nitrogen rather than helium is used in the latest version of AGAS as less-dependent to temperature leaps. The PCS container covered with a protective polyethylene and foam occupies the space around G-12 parachute canopy atop of a standard cargo container (Fig.4b). It is secured to the top of the payload bundle, strapped and tied to the A-22 harness. The PMA fill hoses are taped to the A-22 risers and the riser clevises are tied together with cotton webbing.

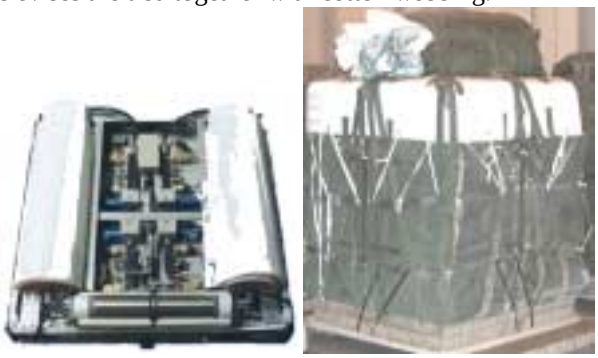

Fig.4 – Vertigo's PCS container (a); and a complete rigged AGAS package ready to fly (b)

* Equilibrium rate of descent is given by the formula $V_d = \sqrt{2mg(C_{D0}S_0\rho)^{-1}}$, where $\rho$ is a mass density of air at desired altitude.

The A-22 harness risers are connected to the Kevlar loops on the bottom ends of the PMAs and the PMA fill hoses are then attached to the PMAs. When these attachments have been tightened and secured, the parachute is lowered onto the top of PCS container. The parachute is tied to the A-22 harness in four places. The flyaway lanyard that arms the AGAS pneumatic system is connected to the parachute deployment bag, then a non-breakaway extraction parachute is attached to the G-12 parachute and the static line is stowed.

The full weight of the AGAS system (including PMAs' control system, tanks, hoses, PMAs, container, batteries, sensor suit, and GNC computer is about 80*kg*. When fully charged with gas the system weights about 11*kg* more.

The GNC electronics package, which is installed into a box in the payload, is connected to the AGAS valve control unit. When the system rigging is complete, the system is pressurized with compressed nitrogen gas and the pneumatic system batteries are charged. The main power switch and main pressure valve remain off until the system is loaded in the aircraft.

II.4. CARP and RT computation

Figures 5 and 6 illustrate the need for the latest available wind profile in the DZ when pre computing RT.

Fig.5 includes plots of the magnitude and direction of the wind measured by eleven Rawinsonde balloons (Fig.7) released at one-hour intervals at the YPG "Tower M" DZ. It is seen that not only magnitude of the wind changes significantly in time, but also that wind may switch directions (see also Ref.38).

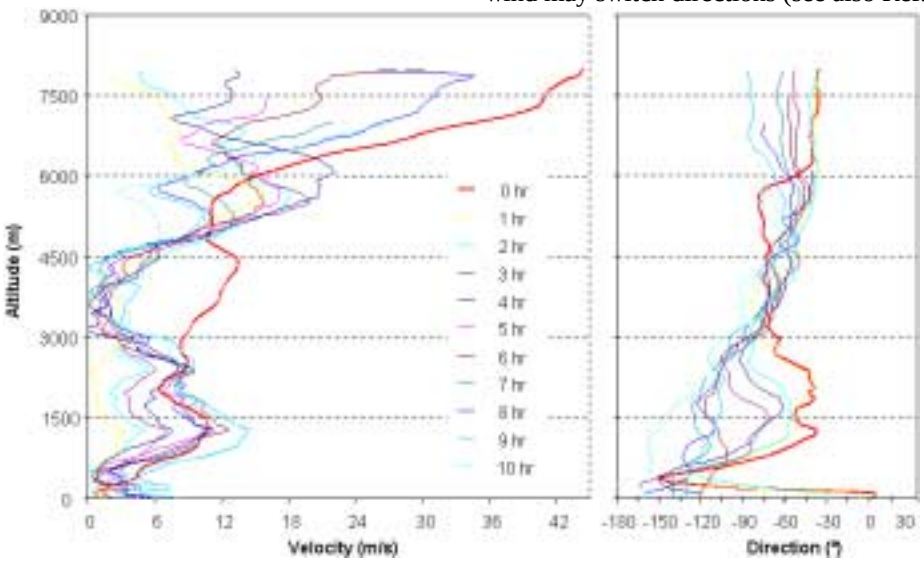


Fig.5 - Measured wind velocity and direction versus altitude

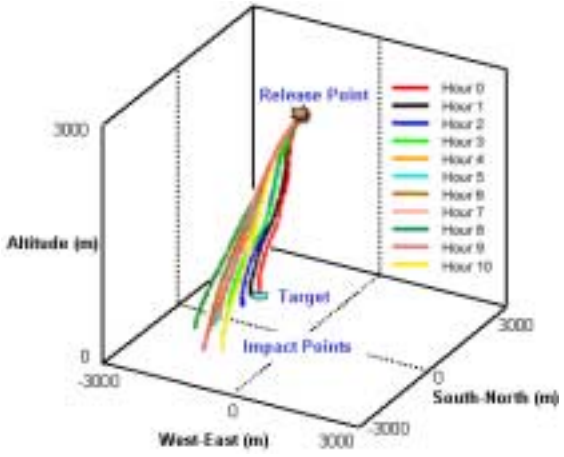


Fig.6 – Uncontrolled trajectories with the different wind profiles

Presently as a part of AGAS effort Draper Labs and Planning Systems Inc. (PSI) developed a highly sophisticated system that provides accurate prognosis of the wind over the DZ to be used for generation of the CARP and the RT[39].

At the moment this system consists of two field laptops. One of them (Planner PC) resides aboard of a C-130 carrier aircraft and is linked to the aircraft's data bus. Its software is designed by Draper Labs to produce CARP and RT and relies on the best available wind profile generated by PSI's software residing on the second WindPADS (Wind-Profile Precision Aerial Delivery System) PC.

Fig.7 - Rawinsonde balloon

To derive preliminary CARP prior to flight, Planner PC is initialized with the set of required data (nominal DZ location, AGAS characteristics including its pay-

load properties, pre-release location of the AGAS in the aircraft cargo bay, aircraft characteristics, nominal payload release altitude, and even the likely uncertainties in the entire input data set). Using an Ethernet connection it also accepts forecast wind and atmospheric density field data over the DZ provided by WindPADS PC. These fields are produced by the 'three-dimensional Mesoscale Model, 5th-generationn (MM5) forecast field' executed on a stationary computer on the ground based on the data provided by the last available Rawinsonde balloon. These high-resolution forecast fields have a horizontal grid spacing of 1.1*km* with appropriately scaled vertical resolution.

The Planner PC's data bus connection is used in a read-only mode to obtain and record aircraft's position, velocity, attitude, and wind-at-altitude data. This data is used to track aircraft location relative to the DZ to enable Planner prediction of the expected time for key events leading up to payload release. The Planner can also accept in-flight user updates to modify the designated TA. This can also be an update provided en route from the ground. When the carrier aircraft nears the DZ at the cruise altitude, a dropsonde is deployed from the carrier aircraft to measure the wind/density profile over/near the DZ following an initial pass through a dropsonde CARP. A transmitted, raw dropsonde RF data signal is received by WindPADS PC through the aircraft UHF antenna, and is processed to produce horizontal wind components as a function of location and time along the dropsonde descent trajectory. The top of the wind profile may also be supplemented with aircraft's wind-at-altitude data produced at the time of dropsonde release.

The updated wind profile near TA is processed in a WindPADS PC's routine that assimilates the new information with the initial MM5 forecast data to produce an accurate, 3D wind and density forecast data set. The Planner PC retrieves this data, produces CARP and RT, and transmits them through a serial port to a wireless transmitter that provides this data set to the AGAS while on-board the carrier aircraft.

In an operational implementation, the Planner PC is supposed to determine a desired approach direction for the CARP, and display corresponding navigation data including flight path to the CARP and time-window prompts for permitted release to the crew.

## III. Synthesis of control algorithms

Based on the AGAS concept introduced above, the optimal control problem for determination of the parachute trajectories from an actual release point (RP) to TA can be formulated as follows: *among all admissible trajectories that satisfy the system of differential equations, given initial and final conditions and constraints on control inputs, determine the optimal trajectory that minimizes a cost function of state variables* $\vec{z}$ *and control inputs* $\vec{u}$

$$J = \int_{t_0}^{t_f} f_0(t, \vec{z}, \vec{u})dt \qquad (1)$$

*and compute the corresponding optimal control.*

For the AGAS, the most suitable cost function *J* is the number of PMA activations. Unfortunately this cost function cannot be formulated analytically in the form given by expression (1). Therefore, we investigated other well-known integrable cost functions and used the results obtained to determine the most suitable cost function for the problem at hand.

To determine the optimal control strategy we applied Pontrjagin's principle[40] to a simplified kinematic planar (3-DoF) model of the parachute. Two possible control schemes are considered in the following subsections. The first one applies directly to the control problem at hand, while the second addresses a possible future control configuration. In each case we consider a no wind scenario. Therefore, the control objective is to steer the parachute to a single stationary point onto a horizontal plane. This is a reasonable approximation of since the control inputs have a negligible effect on the descent rate.

### III.1. Symmetric control

The simplest model describing parachute kinematics in the horizontal plane with four equal on-off controllers may be written as follows (Fig.8):

$$\dot{\vec{P}} = R\vec{U}\ ,\ \dot{\psi} = C + \zeta(t)\ , \qquad (2)$$

where $P = [x, y]^T$ is a state vector, $\vec{U} = [u, v]^T$ - control vector, $R = {}^I_B R$ is a rotation matrix from the body *{B}* to the local tangent plane (LTP) frame *{I}* defined as

$$R = \begin{pmatrix} \cos\psi & -\sin\psi \\ \sin\psi & \cos\psi \end{pmatrix}, \qquad (3)$$

$C = const$ and function $\zeta(t)$ represents disturbances.

This model approximates the impact on the parachute velocity in the lateral plane caused by the activation of each of the four PMAs: $u, v \in [-V; 0; V]$. We consider these speed components as controls for the task at hand.

The Hamiltonian[40] for the system (2) can be written in the following form:

$$H = (p_x, p_y)R\vec{U} + p_\psi(C + \zeta(t)) - f_0\ , \qquad (4)$$

where differential equations for the adjoint variables $p_x$, $p_y$, and $p_\psi$ are given by

$$\dot{p}_x = \dot{p}_y = 0, \quad \dot{p}_\psi = (p_x, p_y)\begin{pmatrix} u\sin\psi + v\cos\psi \\ -u\cos\psi + v\sin\psi \end{pmatrix}. \qquad (5)$$

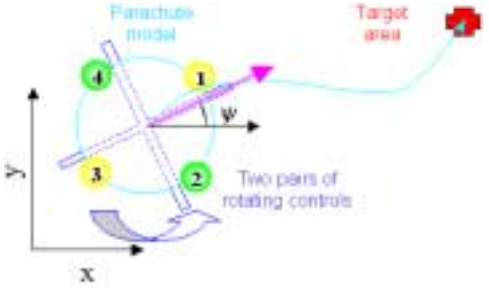


Fig.8 - Projection of the optimization task onto the horizontal plane

We consider two cost functionals

$$f_0 \equiv 1 \text{ and } f_0 \equiv |u| + |v| \qquad (6)$$

usually being used for the minimum-time and minimum fuel problems. Note that in this particular application the second cost function stands for the momentum or energy rather than fuel since AGAS spends gas only to activate PMAs (there is no gas expenditure needed to maintain PMA filled/vented).

Note also that in principle we are looking at the optimal problem with a fixed time (time of descent). However in real life under the actions of atmospheric turbulence and disturbances it would be a good idea to steer parachute to the TA as soon as possible leaving some extra time to fight those disturbances for the rest of the drop.

According to Ref.40, the optimal control is determined as $\vec{u}_{opt} = argmaxH(\vec{p}, \vec{z}, \vec{u})$. Therefore, for the time-minimum problem the optimal control is given by

$$u = Vsign\left( (p_x, p_y) \begin{pmatrix} \cos\psi \\ \sin\psi \end{pmatrix} \right),$$
$$v = Vsign\left( (p_x, p_y) \begin{pmatrix} -\sin\psi \\ \cos\psi \end{pmatrix} \right). \qquad (7)$$

Fig.9 shows the graphical interpretation of these expressions. In general, the vector $(p_x, p_y)$ defines a direction towards the TA and establishes a semi-plane perpendicular to itself that defines the nature of control actions. Specifically, if PMA happens to lie within a certain operating angle (OA) $\Delta$ with respect to the vector $(p_x, p_y)$ it should be activated. For a time-optimum problem $\Delta = \pi$ - therefore, two PMAs will always be active. Parachute rotation determines which two. (We do not address the case of singular control, which in general is possible if the parachute is required to satisfy a final condition for heading.)

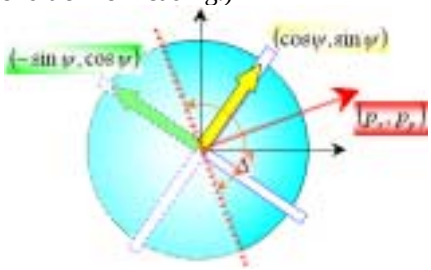


Fig.9 - Time-optimal control

Fig.10 shows an example of time-optimal trajectory. It consists of several arcs and a sequence of actuations. For the sake of simplicity $\dot{\psi} = 2°/s$ was taken for this simulation (as observed in one of the earlier flight-tests).* Maximum horizontal velocity of *V*=3.7*m/s* that corresponds to the data of Tab.2 was used in this example.

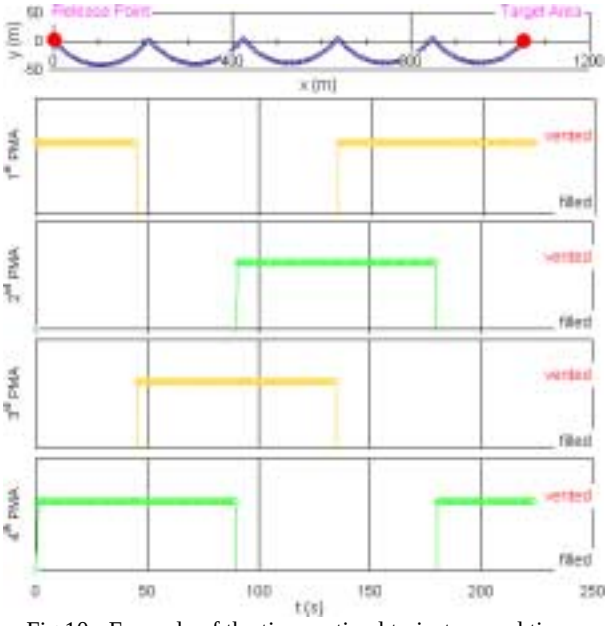


Fig.10 - Example of the time-optimal trajectory and time-optimal controls

For the 'fuel'-minimum problem we obtain analogous expressions for the optimal control inputs:

$$\begin{aligned} p_x \cos\psi + p_y \sin\psi > V &\Rightarrow u = V, \\ p_x \cos\psi + p_y \sin\psi < V &\Rightarrow u = -V, \\ p_x \cos\psi + p_y \sin\psi \equiv V &\Rightarrow u = u_{s.c.}; \\ -p_x \sin\psi + p_y \cos\psi > V &\Rightarrow v = V, \\ -p_x \sin\psi + p_y \cos\psi < V &\Rightarrow v = -V, \\ -p_x \sin\psi + p_y \cos\psi \equiv V &\Rightarrow v = v_{s.c.}. \end{aligned} \qquad (8)$$

In this case PMAs will be employed when an appropriate dot product is greater than some positive value. Obviously, this narrows the OA's magnitude. In fact, for this particular cost function $\Delta \to 0$ #. In general any cost function other than minimum-time will require an operating angle $\Delta \le \pi$ (Fig.11).

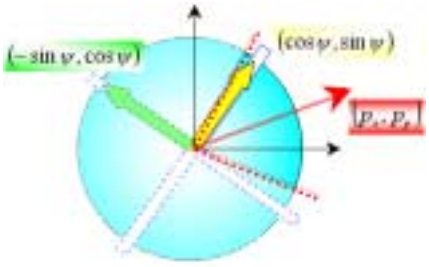


Fig.11 - Generalized case of optimal control

Fig.12 shows the effect of OA's magnitude on the flight time, 'fuel' and number of PMA activations (from 'vented' to 'filled' state). It is clearly seen that the nature of the dependence of the number of actuations on OA is the same as that of the time of flight. This implies that by solving the time-minimum problem we automatically ensure a minimum number of actuations. Moreover, it is also seen that the slope of these

* In principle because of symmetry no rotation should be observed unless any kind of asymmetry is introduced[41].

# Note that any control with $\Delta < 0.5\pi$ may not work at all if parachute is not rotating.

two curves in the interval $\Delta \in [0.5\pi;\pi]$ is flat. This implies that small changes of OA from its optimal value will result in negligible impact on the number of actuations. Therefore, changing the OA to account for the realistic PMA model, as is done on AGAS (see Section IV), will not change the number of actuations significantly.

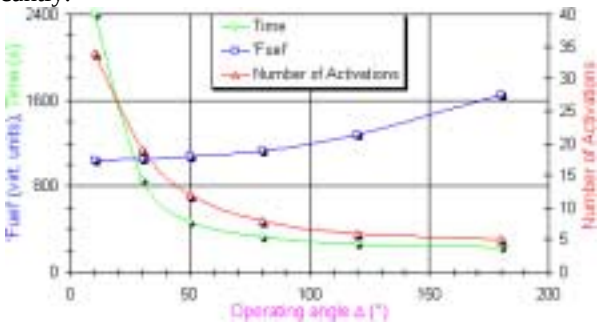


Fig.12 - Influence of OA's magnitude

Fig.13 demonstrates the influence of constant yaw rate on different OA's. The results were obtained for the time optimal control problem illustrated in Fig.10. Obviously, the smaller the yaw rate is, the smaller the number of activations. Decreasing OA for the same yaw rate leads to an increase in the number of PMA activations.

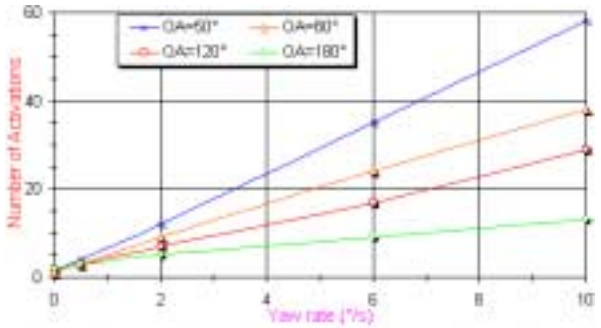


Fig.13 - Influence of a constant yaw rate

Fig.14 includes simulation results for the case where yaw angle from a flight test was used to drive the first two equations in (2) while optimal control was computed using (7). As can be seen the flight test heading is not smooth. Neither is it monotonic. Although a synthesized optimal control drives the model of the parachute towards TA, because of the erratic yaw the number of PMA actuations increases to 35 (versus 12 with the monotonic 2 °/s yaw rate as seen from Fig.12). For this particular simulation OA was equal to 2.5 radians. This example illustrates sensitivity of the optimal control algorithm to uncertainties in heading. Therefore, flight control algorithm must be more robust to these uncertainties to prevent a significant increase in the number of PMA actuations.

III.2. Asymmetric control

We now consider another kinematic model of a parachute in the horizontal plane with the different control architecture[41]. Suppose that after initial deployment and filling of all four PMAs one of them is vented and remains vented throughout the drop. This provides a constant glide ratio (similar to parafoils). Furthermore, suppose that two adjacent PMAs can be half-filled (that means their length could be set as an average between filled and full-vented states). The resulting artificially introduced asymmetry allows us to control parachute's yaw rate. Mathematically, this is expressed by the following simplified equations:

$$\dot{x} = V\cos\psi, \quad \dot{y} = V\sin\psi, \quad \dot{\psi} = v + \zeta(t), \qquad (9)$$

where $v \in [-\Xi;0;\Xi]$ is now the only control (in practice for G-12 based AGAS $\Xi$ would be equal to about 6 °/s).

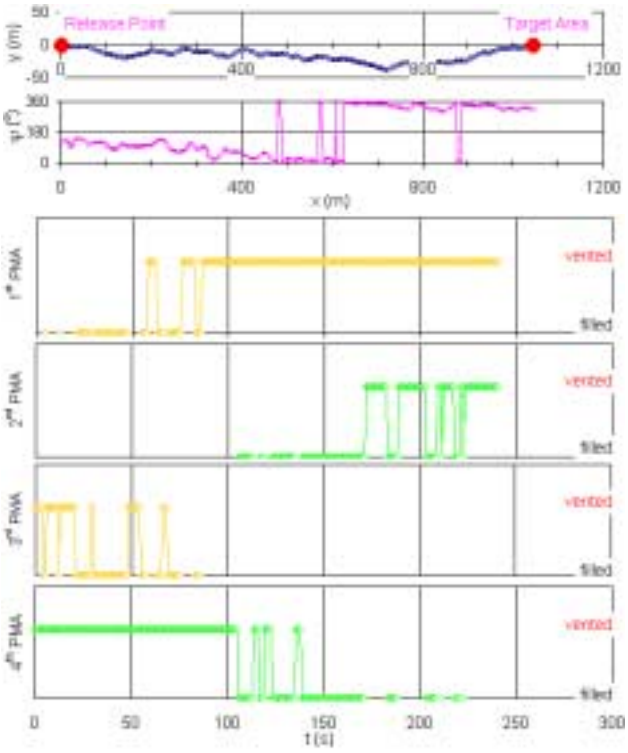


Fig.14 – Flight path computed with usage of a real heading profile

The Hamiltonian for the system (9) can now be written as:

$$H = p_\psi v + V(p_x, p_y)\begin{pmatrix}\cos\psi\\ \sin\psi\end{pmatrix} + p_\psi\zeta(t) - f_0, \qquad (10)$$

where equations for adjoint variables $p_x$, $p_y$ and $p_\psi$ are given by

$$\dot{p}_x = 0, \quad \dot{p}_y = 0,$$
$$\dot{p}_\psi = V(p_x, p_y)\begin{pmatrix}\sin\psi\\ -\cos\psi\end{pmatrix}. \qquad (11)$$

The optimal control for the time-minimum problem now is given by

$$v = \Xi sign(p_\psi). \qquad (12)$$

By differentiating last expression in (11) and combining it with Hamiltonian (10) for both cases when $p_\psi > 0$ and $p_\psi < 0$ we can get a set of equations for $p_\psi$:

$$\ddot{p}_\psi + \Xi^2 p_\psi \mp \Xi = 0. \qquad (13)$$

This differential equation gives two sinusoids (shifted with respect to abscise axis by $\pm\Xi^{-1}$) as solutions for the general (non-singular) case

$$p_\psi = C_1 \sin(\Xi t + C_2) \pm \Xi^{-1}. \quad (14)$$

If $C_1 \neq \Xi^{-1}$ the parachute model moves along a descending spiral. It takes $2\pi\Xi^{-1}$ seconds to make a full turn with a radius of $V\Xi^{-1}$ (that gives ~60*s* and ~40*m* in case of 'modified' AGAS respectively). If $C_1 = \Xi^{-1}$ there exists a possibility of singular control. This is caused by the fact that there exists a point in time where both $p_\psi$ and $\dot{p}_\psi$ are zero as can be seen in (14).

Consider singular control for this model. By definition it means that $p_\psi \equiv 0$. For the time-optimal problem from the Hamiltonian (10) and third equation in (11) (of course keeping in mind the first two) it follows that for a singular control case

$$p_x = V^{-1}\cos\psi, \quad p_y = V^{-1}\sin\psi, \quad \psi = const, \quad (15)$$

Expressions (15) imply that singular control corresponds to motion with constant heading ($v \equiv 0$). It may not however be realized. Instead, the parachute model may switch from right-handed spiral to a left-handed one or vice versa. Planar projections of possible trajectories are shown on Fig.15.

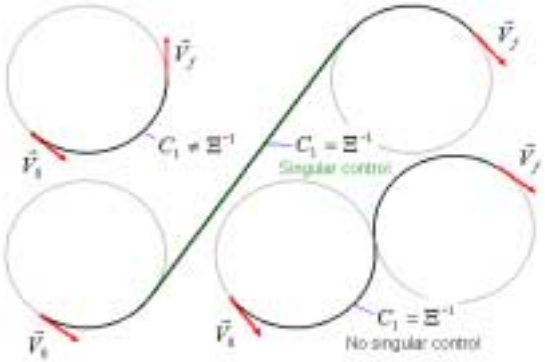


Fig.15 – Possible types of AGAS trajectories in case of potential asymmetric control

The time-optimal trajectories for this case are shown in Fig.16 (trajectories differ by initial orientation of the model). The only PMA actuation is needed in this case to turn parachute velocity vector towards TA at the start.

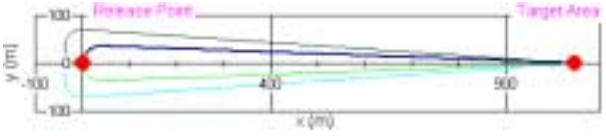


Fig.16 – Modified AGAS model trajectories

To conclude this subsection it worth noting that control algorithms for parafoils (since their control options are quite similar to the discussed above) suggest the same logic consisting of spiral motion in the beginning immediately after deployment followed by straight-line gliding from one way-point to another (if any) towards TA[21-24].

III.3 Optimal control stability

The minimum-time optimal control strategy obtained in the previous section motivates the following feedback control law (7) for the system of equations (2)

$$U = -\,sign(R^T P), \quad (16)$$

where for any vector $\vec{z} \in \Re^n$ we define

$$sign\,\vec{z} = [sign\,z_1, ..., sign\,z_n]^T.$$

It is easy to show using Lyapunov stability theory that this control strategy is globally asymptotically stable. Let

$$L = P^T P \quad (17)$$

denote the Lyapunov function for the feedback system

$$G = \begin{cases} \dot{\vec{P}} = R\vec{U}, \\ \vec{U} = -sign(R^T \vec{P}). \end{cases} \quad (18)$$

Then

$$\dot{L} = P^T \dot{P} + \dot{P}^T P = -\,2P^T R\,sign(R^T P). \quad (19)$$

Since $\vec{z}^T sign\,\vec{z} > 0$, for any nonzero vector $\vec{z}$ and since *R* is a rotation matrix we conclude that

$$\dot{L} < 0, \ \forall P \neq 0.$$

As discussed in Section III the time-optimal control strategy corresponds to the OA of 180°. The same is true for the feedback control strategy (16). Additional design considerations presented in Section IV have resulted in a control strategy with an OA that is less than 180°.

Therefore, in the remainder of this section we propose to analyze stability of a control strategy uses a smaller OA. In order to this, we need to define a new function $sign_\Delta : \Re^n \times \Re^n \to \Re^1$ as follows. Let $\vec{z}_1$ and $\vec{z}_2$ be any two vectors in $\Re^n$. Then

$$sign_\Delta \arg(\vec{z}_1, \vec{z}_2) = \begin{cases} 1, & \arg(\vec{z}_1, \vec{z}_2) \le \dfrac{\Delta}{2}, \\ 0, & |\arg(\vec{z}_1, \vec{z}_2) - \dfrac{\pi}{2}| < \dfrac{\Delta}{2}, \\ -1, & \text{otherwise.} \end{cases} \quad (20)$$

Now using (20) we define the feedback control strategy (see Fig.17)

$$U = \begin{cases} \left[ \begin{array}{c} -sign_\Delta \arg\left( \dfrac{R^T P}{\|R^T P\|}, \begin{bmatrix} 1 \\ 0 \end{bmatrix} \right) \\ -sign_\Delta \arg\left( \dfrac{R^T P}{\|R^T P\|}, \begin{bmatrix} 0 \\ 1 \end{bmatrix} \right) \end{array} \right], P \neq 0, \\ 0, \ \text{otherwise.} \end{cases} \quad (21)$$

Clearly, for $\Delta = \pi$ (21) reduces to (16). Let the Lyapunov function *L* be defined in (17). Then

$$\dot{L} = -2P^T R \begin{bmatrix} -sign_\Delta \arg\left(\dfrac{R^T P}{\|R^T P\|}, \begin{bmatrix}1\\0\end{bmatrix}\right) \\ -sign_\Delta \arg\left(\dfrac{R^T P}{\|R^T P\|}, \begin{bmatrix}0\\1\end{bmatrix}\right) \end{bmatrix}. \quad (22)$$

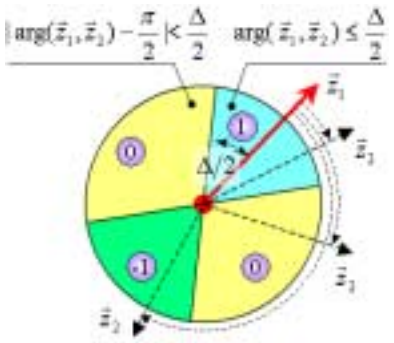


Fig.17 – Explanation of control strategy in terms of function (20)

Define a function $sign_\varepsilon : \Re^1 \to \Re^1$ analogous to (20)

$$sign_\varepsilon a = \begin{cases} 1, & a \ge \varepsilon, \\ 0, & |a| < \varepsilon, \\ -1, & a \le -\varepsilon. \end{cases}$$

Let $a_1 = \left(\left(\dfrac{R^T P}{\|R^T P\|}\right)^T, \begin{bmatrix}1\\0\end{bmatrix}\right)$, $a_2 = \left(\left(\dfrac{R^T P}{\|R^T P\|}\right)^T, \begin{bmatrix}0\\1\end{bmatrix}\right)$,

and $\varepsilon = \cos(\dfrac{\Delta}{2})$.

Then (see Fig.18) $sign_\Delta \arg\left(\dfrac{R^T P}{\|R^T P\|}, \begin{bmatrix}1\\0\end{bmatrix}\right) = sign_\varepsilon a_1$,

$sign_\Delta \arg\left(\dfrac{R^T P}{\|R^T P\|}, \begin{bmatrix}0\\1\end{bmatrix}\right) = sign_\varepsilon a_2$ and $R^T P = \|R^T P\| \begin{bmatrix} a_1 \\ a_2 \end{bmatrix}$.

Furthermore, for $\forall P \ne 0$

$$\dot{L} = -2\|R^T P\| \begin{bmatrix} a_1 & a_2 \end{bmatrix} \begin{bmatrix} dsign_\varepsilon a_1 \\ dsign_\varepsilon a_2 \end{bmatrix} = C\|R^T P\|, \quad (23)$$

where

$$C = \begin{cases} -4, & a_1 \ge \varepsilon \,\&\, a_2 \ge \varepsilon \vee a_1 \le -\varepsilon \,\&\, a_2 \le -\varepsilon, \\ -2, & -\varepsilon < a_1 < \varepsilon \,\&\, a_2 \ge \varepsilon \vee a_1 \ge \varepsilon \,\&\, -\varepsilon < a_2 < \varepsilon, \\ -2, & -\varepsilon < a_1 < \varepsilon \,\&\, a_2 \le -\varepsilon \vee a_1 \le -\varepsilon \,\&\, -\varepsilon < a_2 < \varepsilon, \\ 0, & |a_1| < \varepsilon \,\&\, |a_2| < \varepsilon. \end{cases}$$

Last expression indicates that the candidate Lyapunov function $L = P^T P$ does not guarantee asymptotic stability for the feedback control strategy (21) when $|a_1| < \varepsilon$ and $|a_2| < \varepsilon$. As illustrated in Fig.18, this situation can occur only when $\Delta < 0.5\pi$.

Therefore, the feedback strategy (21) guarantees global asymptotic stability in the sense of Lyapunov for any $\Delta \ge 0.5\pi$.

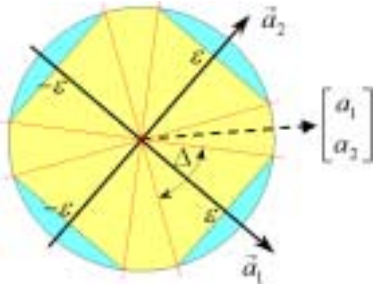


Fig.18 – Possibility of absence of asymptotic stability

## IV. Flight control algorithm

As discussed in Section II the actuation box for PMA's developed by Vertigo is capable of only bang-bang control. Optimal control analysis of a simplified parachute model discussed in Section III suggested that bang-bang is also the optimal control strategy and produced an important concept of an operating angle. This motivated the following basic control concept for AGAS. Since the time-optimal control strategy was shown to minimize the number of actuations for a planar model this strategy was employed to get the parachute to within a predefined altitude-dependent TA (defined by inner and outer cones discussed next) and then for the remainder of descent to stay within this area. In addition, this basic strategy must be robust to uncertainties in yaw motion. These considerations were used to develop the flight control algorithm for AGAS and are detailed next.

### IV.1.Basic control architecture

Considering the relatively low glide ratio demonstrated in flight test (see Tab.2) AGAS can only overcome less than 4*m/s* wind. It is therefore imperative that the control system steers the parachute along a pre-specified RT obtained from most recent wind prediction. This can be done by comparing the current GPS position of the parachute with the desired one on RT at a given altitude to obtain the position error

$$\vec{P}_e(h) = \vec{P}_{AGAS}(h) - \vec{P}_{CARP}(h). \quad (24)$$

This position error $\vec{P}_e(h)$ is computed in LTP frame with an origin in the TA and is then converted to the body axis using an Euler angle rotation $R^T$ computed using yaw angle only (3). The resulting body-axis error vector

$$\vec{P}_B = R^T \vec{P}_e \quad (25)$$

is then used to identify error angle (EA)

$$EA = \arg \vec{P}_B. \quad (26)$$

In turn EA is then used to define what PMA ($i = 1,...,4$) must be activated:

$$i=\begin{cases}1, & if \quad EA\le\dfrac{\Delta}{2}\vee EA\ge 2\pi-\dfrac{\Delta}{2},\\ 2, & if \quad EA\in\left[\dfrac{3\pi}{2}-\dfrac{\Delta}{2};\dfrac{3\pi}{2}+\dfrac{\Delta}{2}\right],\\ 3, & if \quad EA\in\left[\pi-\dfrac{\Delta}{2};\pi+\dfrac{\Delta}{2}\right],\\ 4, & if \quad EA\in\left[\dfrac{\pi}{2}-\dfrac{\Delta}{2};\dfrac{\pi}{2}+\dfrac{\Delta}{2}\right]\end{cases} \qquad (27)$$

(by definition EA is counted from PMA #3 counter-clockwise, i.e. in the situation shown as example on Fig.19 PMAs #2 and #3 would be activated (vented).

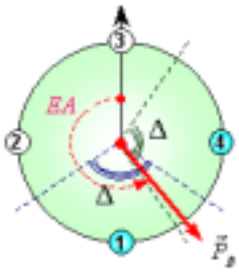


Fig.19 – Control-activation rule

In order to account for the refill time and sensors errors the operating angle was set to $\Delta\approx 2.5$ radians instead of $\Delta=\pi$ [*]. This still allows the activation of a single control input or two simultaneous control inputs without significant degradation of AGAS performance (see Fig.12).

IV.2. Outer and inner cones

First of all, the initial error after deployment should not exceed a certain value because of AGAS' limited control authority. This area of attraction has the radius $R_A$ around RT that can be roughly estimated by a simple formula

$$R_A(h)=0.8k_\Delta GR_{\max}h\text{, where } k_\Delta\approx\Delta\pi^{-1}. \qquad (28)$$

Coefficient $k_\Delta$ is approximated by using the data of Fig.12, and coefficient 0.8 accounts for real-world yaw profile.

To eliminate unnecessary actuations of PMAs a tolerance (outer) cone was established (Fig.20). Its radius at CARP (at an altitude of $3000m$) is $\Re_{outer}(3000)=200m$ -radius and it decreases linearly to $\Re_{outer}(0)=100m$ -radius circle at the TA (at ground level). Should the magnitude of the position error in the lateral plane $\left|\vec{P}_B(h)\right|$ be outside of this tolerance cone

$$\left|\vec{P}_B(h)\right|>\Re_{outer}(h), \qquad (29)$$

a control is activated to steer the system back to the planned RT.

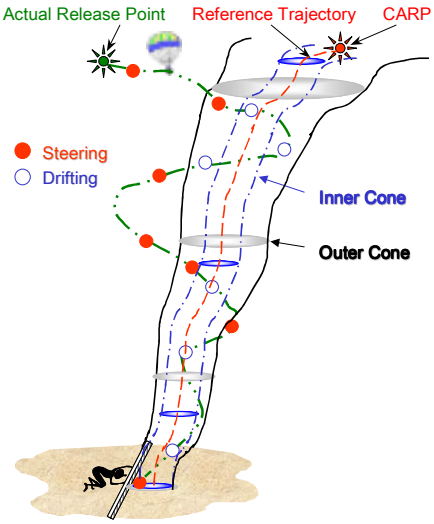


Fig.20 - Outer and inner cones

When the system is within the inner cone $\Re_{inner}$

$$\left|\vec{P}_B(h)\right|<\Re_{inner}, \qquad (30)$$

(which is set to $60m$-radius regardless of altitude) the control is disabled and the parachute drifts with the wind ($\Re_{inner}$ was selected to account for the refill time) until outer cone is reached and control is activated again.

The basic control strategy uses the following **activation rule**: both the tolerance cone and the operating angle constraints must be active for a given PMA to be actuated.

IV.3. Robustness issues

The control algorithm outlined above was flight tested at YPG. As expected the number of PMA actuations was unacceptably high. This resulted in a premature emptying of PCS tanks. Analysis of flight test data indicated that this was caused by frequent heading changes and that that these changes occurred when one of the adjacent PMAs was actuated while the other one was in transition from vent to full or vice versa.

Fig.21 explains this phenomenon. If one PMA is activated (vented) and adjacent PMA is performing a transition from one state to another this causes a yaw moment $\vec{M}_c$. This moment can be 'useful' (when the direction of rotation of the vector $\vec{P}_B$ is opposite to the direction of $\vec{M}_c$), or harmful (vise versa). In the latter case the rotation of the parachute under the action of $\vec{M}_c$ causes a deactivation command to the PMA that was just activated. Moreover during this deactivation the 'useful' moment in turn makes situation even worse. This case is shown on Fig.22a.

[*] On the earliest AGAS versions refill time was not constant and was equal to about $20sec$ at the end, that for the yaw rate of 2 °/s gives around 40°.

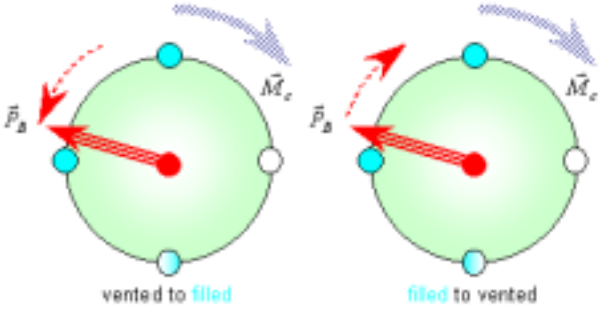

Fig.21 – 'Positive' (left) and negative effect of PMA transition moment

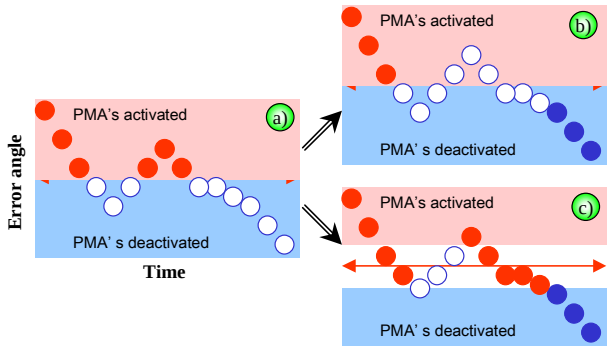

Fig.22 - Two ways of decreasing the influence of yaw oscillations

To eliminate unnecessary activations delay logic in each PMA channel was introduced. Any new command that requires change in the PMA state triggers the delay timer. While the delay timer is active no command is executed including the triggering command. At the end of the delay the timer is reset and the first available command is executed until the next command that requires change in the PMA state triggers the delay timer again.

The number of unnecessary actuations can also be reduced by introducing hysteresis as shown on Fig.22c.

Both delay and hysteresis angle values can be adjusted as a function of system dynamics and in principle achieve the same result.

## IV.4. Prediction term

Another approach that drastically improves robustness in the presence of yaw oscillations is to introduce a derivative term into the control logic (25) as follows.

First, change inequalities (29) and (30) to

$$\left|R^T\left(\vec{P}_e - k_c\dot{\vec{P}}_e\right)\right| > \Re_{outer}\ ,\ \left|R^T\left(\vec{P}_e - k_c\dot{\vec{P}}_e\right)\right| < \Re_{inner}\ . \quad (31)$$

where coefficient $k_c$ should be adjusted to provide better performance (smallest overshoot). This softens outer and inner cone edges. For example if AGAS is approaching the inner cone with high planar velocity rather than slowly drifting into it is better to deactivate (fill) all PMAs earlier than would be done by the control strategy based on (30). On the other hand, if AGAS is leaving the outer cone with high planar velocity it is worth activating (venting) an appropriate PMA(s) to prevail further rapid increase of the radial error earlier than would be done by (29).

Second redefine EA to be

$$EA = \arg\left\{R^T\left(\vec{P}_e + k_r\dot{\vec{P}}_e\right)\right\}. \quad (32)$$

where $k_r$ determines the delay in the execution of next command prescribed by (27) similar to the one discussed in the previous section. Compare definition of EA in (32) with that in (26).

Notice, that expressions (31) and (32) have opposite signs for the derivative term. In (31) the negative sign accelerates control action, whereas in (32) it does the opposite therefore reducing sensitivity to the oscillations in yaw.

## IV.5. Bad wind accounting

For the case when available wind prediction is either too old or non-existent an alternative to tracking an RT is proposed. When latter is true Eq.(24) becomes

$$\vec{P}_e(h) = \vec{P}_{AGAS}(h)\ . \quad (33)$$

On the other hand when wind prediction is available we propose use

$$\vec{P}_e(h) = \vec{P}_{AGAS}(h) - \vec{P}_{CARP}(k_w h)\ , \quad (34)$$

to define $\vec{P}_e(h)$ ,where $k_w \in [0;1]$ represents wind estimate quality (0 - poor, 1 - excellent).

Appropriate value of $k_w$ can be determined by comparing real-time motion of AGAS during a drop with its predicted response generated by the onboard model. In fact, assuming the model is sufficiently accurate it can be used to determine errors in the predicted wind profile.

## IV.6. Deployment delay

As a safety precaution the GNC system starts implementing control commands 25 seconds after initial deployment. This time is needed for AGAS to be released, for main canopy to be fully deployed and for risers to untwist as shown on Fig.23.

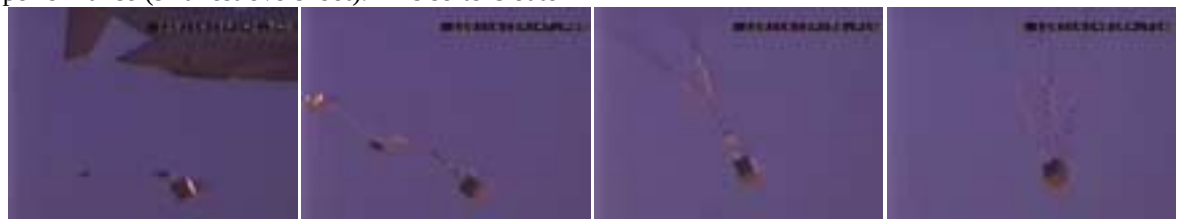
Fig.23 - AGAS deployment and risers untwisting sequence

By design the initial shock during deployment is absorbed by 6-ton Kevlar load lines. So all PMAs are initially vented (when vented they are longer than Kevlar load lines). The first command sent and executed after 25-second deployment delay is to fill all PMAs (as shown of Fig.24). After additional 5*sec* any other command can be executed.

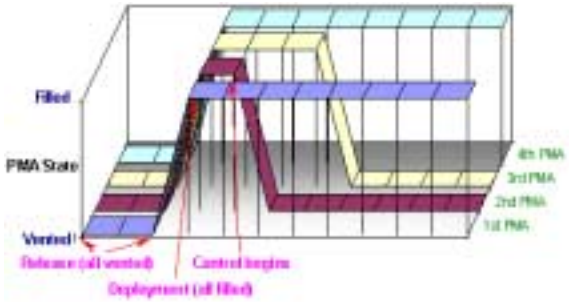


Fig.24 – Control actions history right after release

## V. Non-linear simulation results

### V.1. AGAS model

The control algorithm discussed in Section IV was first tested in a simulation environment using an AGAS model developed in Ref 28. This model assumes low speed descent (with the main canopy fully deployed) and is a complete nonlinear 6-DoF model of a controlled G-12 parachute. This simulation also included models of PMA's dynamics. Fig.25 shows an example where the 3D position of AGAS from a flight test is compared to that generated by the model. The model output matches flight test data fairly well with only 15*m*-difference between impact points (IPs). Number of PMA actuation is the same and is equal to 14.

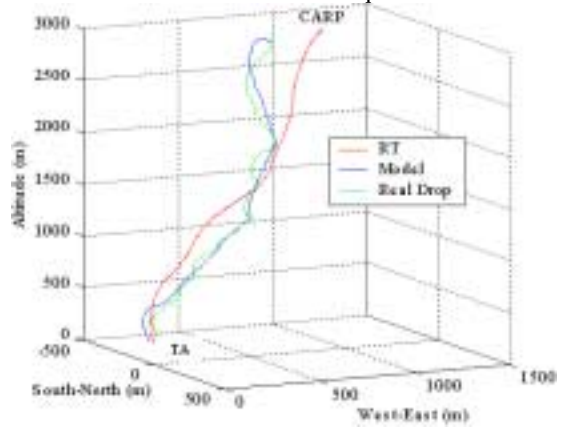


Fig.25 – AGAS model versus real AGAS drop

### V.2. Simulation analysis

Extensive simulation analysis was done to test the flight control algorithm, to produce accuracy requirements for the sensor suite and control authority requirements for PCS and to estimate AGAS overall performance. Some of these results are given below.

Fig.26 for instance shows the result of Monte Carlo simulation that verifies the general AGAS concept and demonstrates overall performance of the AGAS control algorithm for a variety of wind profiles, release altitudes and sensor errors artificially introduced into the model. Clearly, the developed control algorithm performs well in all the cases considered here.

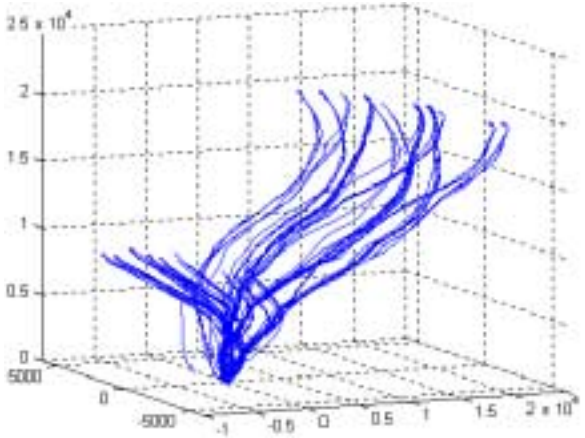

Fig.26 - Monte Carlo simulation

Fig.27 illustrates the influence of OA's magnitude on control performance. In this case only the basic control algorithm was tested, i.e. there were no cones, delay, hysteresis or any other additional features designed to minimize the number of actuations discussed in the previous section were included. Each graph represents radial error versus current altitude during the simulated drops. The target is at (0,0) on the graph.

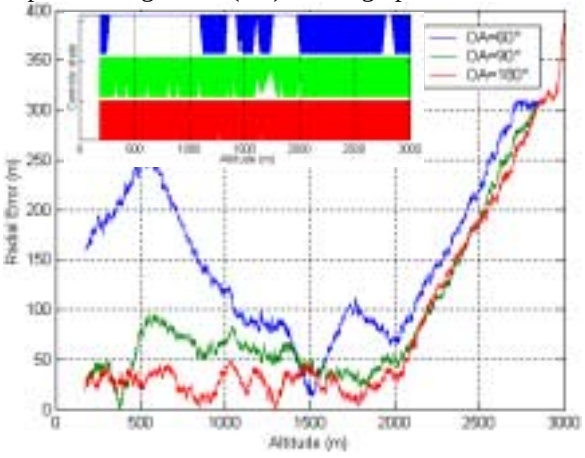


Fig.27 – Simulations with different OAs

While simulation with OA=180° ensures the best accuracy of pre-defined RT tracking it also requires 53 actuations*. With the decrease of OA the number of activations also decreases (17 for $\Delta = 90°$ and 14 for $\Delta = 60°$). However touch down accuracy degrades as well.

The top-left portion of Fig.27 shows when any of PMAs was activated during simulation with each OA. Obviously with $\Delta < 90°$ blind sectors with no PMA activation becomes possible (i.e., $\Delta < 90°$ does not handle the control).

Fig.28 illustrates the impact of introducing outer and inner cones on the control performance. The operating angle in this simulation and hereafter was $\Delta = 143°$ and

* Compare it with 35 activations obtained in simulation with the sane yaw profile on Fig.14 when using 3-DoF model.

the number of actuations was nine (as opposed to 24 without cones). Obviously this was achieved by not activating PMAs while between cones (see the band-type graph similar to one on Fig.27 in the center of Fig.28).

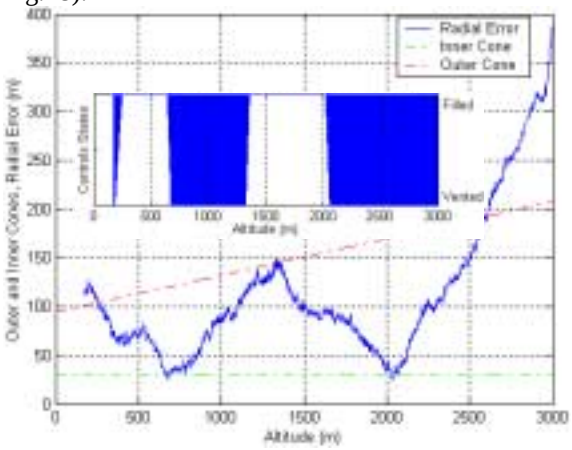


Fig.28 – Introducing the cones

Although nine activations seem to be an excellent result (for considered CARP based on very good knowledge of a real wind profile) the analysis revealed that almost half of them was due to yaw oscillations. As discussed in the previous section to reduce unnecessary activations is by introducing delay or hysteresis. Fig.29 gives an idea of how these features affect performance of the system. It was also revealed that while the delay does not affect the number of PMA actuations (for this simulation it remained approximately the same nine, nine and ten for 0, 5 and 10*sec* delay respectively), the hysteresis not only improves performance but decreases the number actuations as well: nine for 0º, and 5 for ±5º and ±10º. Because of this all further simulations included hysteresis of ±5º.

Fig.30 shows the effect of introducing a prediction term (31). As expected the overall performance improves (trajectory stays strictly between cones). However obviously this term leads to a certain increase of number of PMA activations (dead zone between two 'soft-edge' cones is smaller then between 'solid-edge' ones). For this particular simulation the number of activations was equal to five with no prediction, 10 with 5…10*sec* prediction and 14 with $k_c = 20sec$.

Fig.31 summarizes the previous discussion and shows the decrease of total number of PMA activations when more sophisticated control logic is employed. As seen, we managed to decrease sufficiently the number of PMA activations in comparison with the basic 'classical' term ensuring almost septuple reserve with respect to available control authority (34 activations).

Finally, Fig.32 includes results of a simulation where $\vec{P}_e$ is defined using (33) also known as target-seek control strategy. These results are compared with the standard RT-tracking strategy (24). All inputs are the same for both simulations including $\Delta = 143°$, 'solid-edge' cones (around RT in the first case and around vertical line stretching upward from the target), and ±5º hysteresis. No-control trajectory is shown also. Both algorithms perform well requiring only five PMA activations each.

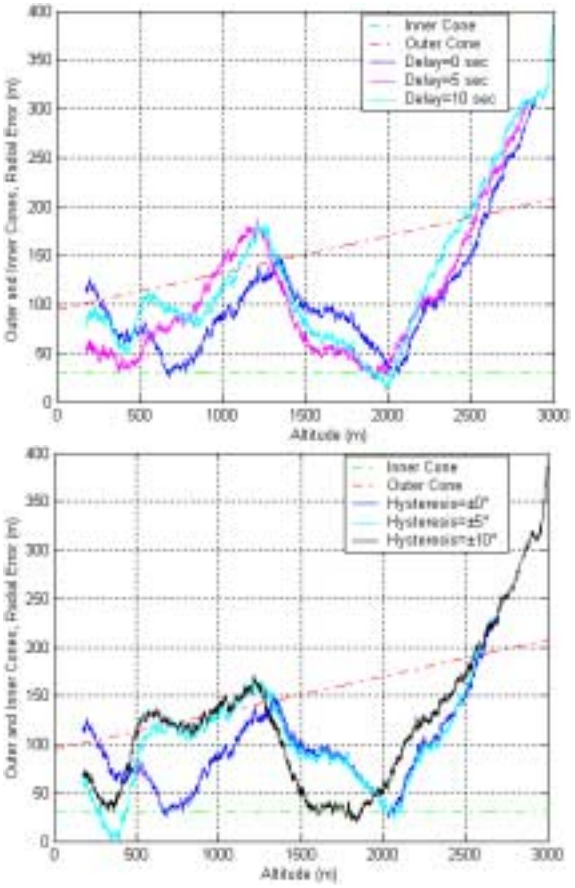


Fig.29 – Introducing delay and hysteresis to fight yaw oscillations

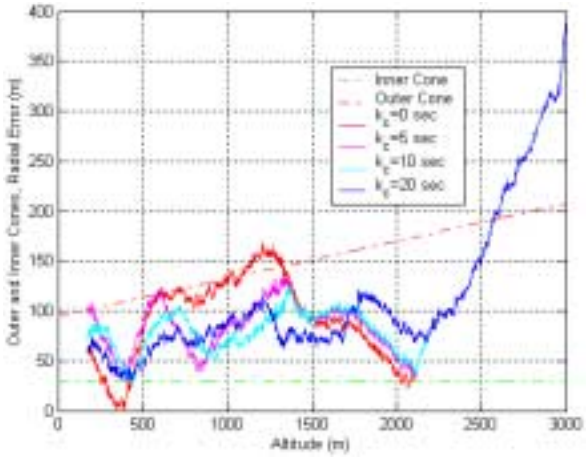


Fig.30 – Introducing a prediction term

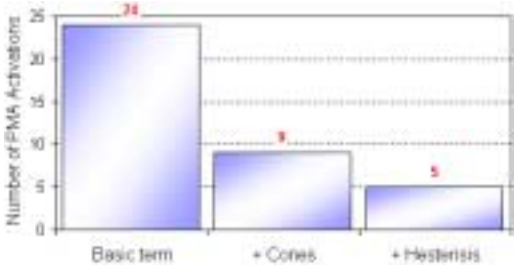


Fig.31 – Number of PMAs activations decrease

Fig.32 also shows the real wind profile during the drop. First observe that the release point does not coincide with the CARP (about 300*m* difference). For the first 2000*m* of altitude the prediction of wind (RT) differs form the real wind profile insignificantly (accruing about 50*m* difference in position). But for the rest of the drop the difference gradually increases making over 350*m* at the touchdown point. So we may say that during this simulation the predicted wind profile was far away from the real one. However a reasonable algorithm suggested by (33) handled this situation fairly well.

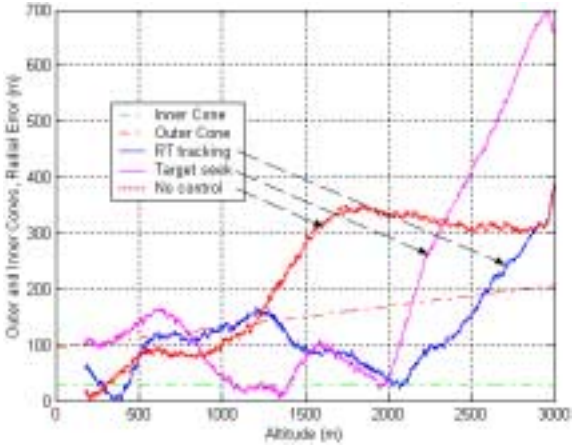


Fig.32 – RT-tracking versus Target-seek trajectories

## VI. Flight test

A total of about 15 controlled drops were made at YPG to test the AGAS concept. The final demonstration took place at YPG during Precision Airdrop Technology Conference and Demonstration (PATCAD) on September 13th and 14th 2001[31].

During preliminary tests a ground station was used to control AGAS via a wireless modem[29]. The AGAS sent its current position and heading to the ground station, the ground station processed the data using the flight control algorithm and then issued appropriate commands to the AGAS GNC.

For the final drops all GNC algorithms were executed aboard AGAS. The downlink message was used for real-time monitoring during the drop.

The rest of the paper describes a pre-flight procedure, flight test setup and the results of two successful drops of four AGAS performed during the final PATCAD demonstration.

### VI.1. Flight test setup

According to the general procedure after AGAS had been rigged, pressurized, and charged, it was taken to the scales to be weighed, and a communication link check was also performed. Next, the system was loaded onto the aircraft and the main valve was opened.

When the aircraft was at a drop altitude and before it started its cold pass over the DZ, the main power switch was turned on and the GNC hardware was armed. As the plane arrived at the CARP, the AGAS system was deployed, as well as a door-deployed wind-pack bundle that was weighted to descend at the same rate as the AGAS system (to provide real wind profile during the drop for the future analysis).

Fig.33 shows the sequence of deployment during PATCAD demonstration. To make the difference between non-controlled and controlled parachute more clear two standard G-12 and two AGAS (followed by the wind-pack) were deployed simultaneously.

Fig.33 - Deployment sequence

After landing (Fig.34) everything was checked, rigged again and prepared for the next drop.

Fig.34 - After the drop

### VI.2. Flight data analysis

Several same-weight category systems including both circular parachutes and parafoils were demonstrated at PATCAD. AGAS performed better than others. The miss distance for the four AGAS systems released was less than 78*m* as oppose to 140…1370*m* for uncontrolled parachutes (see Tab.3).

Tab.3. PATCAD results

| Date | Test Item | Weight *(kg)* | IP miss (*m*) |
|---|---|---|---|
| 09/13/01 | *WindPack* | 21 | 515.1 |
| | *STD G-12* | 724 | 512.2 |
| | *STD G-12* | 773 | 141.9 |
| | ***AGAS-1*** | **726** | **76** |
| | ***AGAS-2*** | ***726*** | ***78*** |
| 09/14/01 | *WindPack* | 21 | 1048.6 |
| | *STD G-12* | 726 | 1371.6 |
| | ***AGAS-3*** | **726** | **347.3*** |
| | ***AGAS-4*** | **726** | **55.5** |

* On September 14th AGAS-3 quit working half the way down because of valve system malfunction.

Fig.35 shows that the same control algorithm being employed at two AGAS led to impact of two systems during the first drop. For the second drop different TA were input into the GNC systems of two parachutes to avoid possible collision.

Fig.35 - Two AGAS steering towards CARP

Fig.36 demonstrates the integral data for two first-day drops from the altitude of 3000*m*. The 30-*min* old wind data was used to compute the RT. It is seen that regardless a large initial error both AGAS steered to the TA fairly well: 17 and 18 PMA activations were needed to hit the target with approximately the same miss distance.

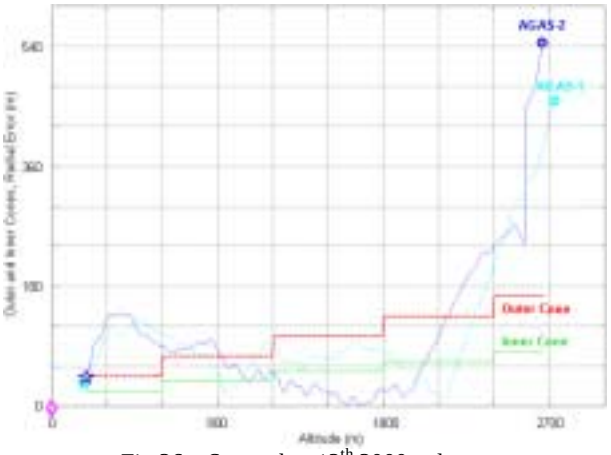


Fig.36 – September 13th 3000*m* drops

Fig.37 presents the same kind of data for the second set of AGAS on September 14th (released at 5000*m*). The wind profile used for this drop was two hours old. Observe that in spite of coincidence of the AGAS-4 actual release point with its CARP because of bad wind estimate parachute drifts out of RT for the first 1000*m*. However upon leaving the outer cone it is steered back inside. As soon as the PMAs inflate upon entering the inner cone the AGAS proceeds to drift out again.

Fig.38 shows the control-related data for the AGAS-4. 28 PMA fills were needed to hit the target with a 55*m* miss.

## VII. Conclusions

Results presented in this paper showed feasibility of the AGAS concept. A bang-bang control strategy imposed by the PMA hardware was developed to successfully drive AGAS to TA within prescribed circular error in flight tests at YPG. The key to the success of this strategy were concepts of operating angle motivated by optimal control analysis as well as inner and outer cones and hysteresis included to improve performance robustness.

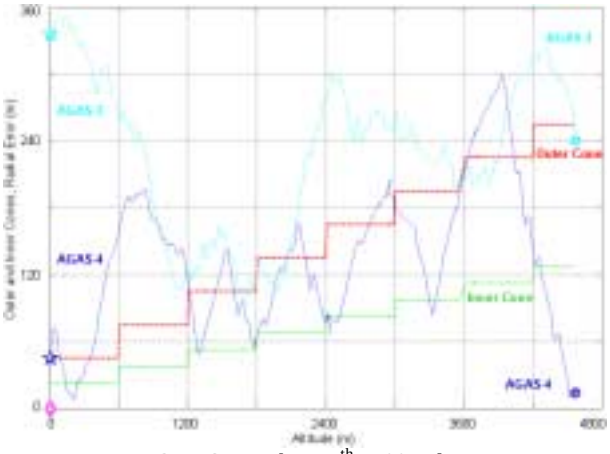


Fig.37 – September 14th 4500*m* drops

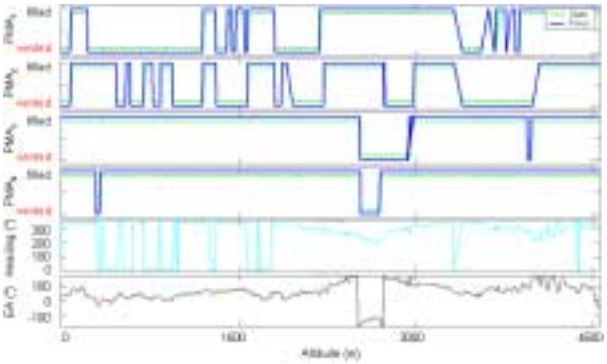

Fig.38 – AGAS-2 control data


## Acknowledgements

Authors are thankful to YPG team members as well as to Vertigo, Inc., Draper Labs and PSI, Inc. team members for their help with the flight test setup. We would also like to thank NPS graduate students participated in the earliest stages of the project (modeling).


## References


1. "Summary Report: New World Vistas, Air and Space Power for the 21st Century," *United States Air Force Science Advisory Board*, 1997.
2. Brown, G., Haggard, R., Almassy, R., Benney, R., and Dellicker, S., "The Affordable Guided Airdrop System," *15th CAES/AIAA Aerodynamic Decelerator Systems Technology Conference*, Toulouse, France, June 9-11, 1999.
3. Dellicker, S., and Bybee, J., "Low Cost Parachute Guidance, Navigation, and Control," *15th CAES/AIAA Aerodynamic Decelerator Systems Technology Conference*, Toulouse, France, June 9-11, 1999.
4. Tory, C. and Ayres, R., "Computer Model of a Fully Deployed Parachute," Journal of Aircraft, Vol.14, No.7, 1977, pp.675-679.
5. Eaton, J.A., and Cockrell, D.J., "The Validity of the Leicester Computer Model for a Parachute with Fully-Deployed Canopy," *Proceedings of 6th AIAA Aerodynamic Decelerator and Balloon Technology Conference*, Houston, TX, March 5-7, 1979.
6. Cockrell, D.J. and Doherr, K.-F., "Preliminary Consideration of Parameter Identification Analysis from Parachute Aerodynamic Flight Test Data," *Proceedings of 7th AIAA*

*Aerodynamic Decelerator and Balloon Technology Conference*, San Diego, CA, October 21-23, 1981.
7. Eaton, J.A., "Added Mass and the Dynamic Stability of Parachutes," *Journal of Aircraft*, Vol.19, No.5, 1982, pp.414-416.
8. Antonenko, A., Rysev, O., Fatyhov, F., Churkin, V., and Yursev, Y., "Flight Dynamics of Parachute Systems," *Mashinostroenie*, Moscow, 1982 (in Russian).
9. Shevljakov, Y., Temnenko, V., and Tischenko, V., "Dynamics of Parachute Systems," Vischa Shcola, Odessa 1985 (in Russian).
10. Rysev, O., Belozerkovsky, S., Nisht, M., and Ponomarev, A., "Parachutes and Hang-Gliders Computer Investigations," *Mashinostroenie*, Moscow, 1987 (in Russian).
11. Doherr, K.-F., and Schilling, H., "Nine-Degree-of-Freedom Simulation of Rotating Parachute Systems," *Journal of Aircraft*, Vol.29, No.5, 1992, pp.774-781.
12. Doherr, K.-F., "Parachute Flight Dynamics and Trajectory Simulation," *Patrachute Systems technology Short Course*, University of Minnesota, October 26, 1994.
13. Heinrich, H.G. and Haak, E.L., "Stability and Drag of Parachutes with Varying Effective Porosity," *Wright-Patterson AFB*, ASD-TDR-62-100, Sept. 1962.
14. White, F.M., and Wolf, D.F., "A Theory of Three-Dimensional Parachute Dynamic Stability," *Journal of Aircraft*, Vol.5, No.1, 1968, pp.86-92.
15. Shilov, A.A., "An Analysis of the Plane Slightly-Dumped Oscillation of a Parachute in Free Steady Descent," FTD-MT-465-75, *Uchenie zapiski TsAGI*, vol.2, No.4, pp76-83, 1971 (in Russian).
16. Shilov, A.A., "The Stability of Motion of Parachute in Steady State Reduction Mode", FTD-MT-24-510-75, *Uchenie zapiski TsAGI*, vol.4, No.1, pp. 137-143, 1973 (in Russian).
17. Doherr, K.-F., "Theoretical and Experimental Investigation of Parachute-Load-System Dynamic Stability," *Proceedings of 5th AIAA Aerodynamic Decelerator and Balloon Technology Conference*, Albuqurque, NM, 1975.
18. Yavus, T., and Cockrell, D.J., "Experimental Determination of Parachute Apparent Mass and Its Significance in Predicting Dynamic Stability," *Proceedings of 7th AIAA Aerodynamic Decelerator and Balloon Technology Conference*, San Diego, CA, October 21-23, 1981.
19. Doherr, K.-F., and Saliaris, C., "On the Influence of Stochastic and Acceleration Dependent Aerodynamic Forces on the Dynamic Stability of Parachutes," *Proceedings of 7th AIAA Aerodynamic Decelerator and Balloon Technology Conference*, San Diego, CA, October 21-23, 1981.
20. Cockrell, D.J., and Haidar, N.I.A., "Influence of the Canopy-Payload Coupling on the Dynamic Stability in Pitch of a Parachute System," *Proceedings of 12th RAeS/AIAA Aerodynamic Decelerator Systems Technology Conference and Seminar*, London, England, May 10-13, 1993.
21. Forehand, J.E., "The Precision Drop Glider (PDG)," *Proceedings of the Symposium on Parachute Technology and Evaluation*, El Centro, CA, April 1969 (USAF report FTC-TR-64-12, pp.24-44).
22. Wailes, W., and Hairington, N., "The Guided Parafoil Airborne Delivery System Program", *13th AIAA Aerodynamic Decelerator Systems Technology Conference*, Clearwater Beach, FL, May 15-18,1995.
23. Smith, B.D., "Steering Algorithms for GPS Guidance of RAM-AIR Parachutes," *Proceedings the 8th International Technical Meeting of the Institute of Navigation (IONGPS-95)*, Palm Springs, CA, September 12-15, 1995.
24. Final Report: Development and Demonstration of a Ram-Air Parafoil Precision Guided Airdrop System, Volume 3, *Draper Laboratory* under Army Contract DAAK60-94-C-0041, October 1996.
25. Dellicker, S., "Low Cost Parachute Navigation Guidance and Control," MS thesis, *Naval Postgraduate School*, September 1999.
26. Williams, T., "Optimal Parachute Guidance, Navigation, and Control for the Affordable Guided Airdrop System (AGAS)," MS thesis, *Naval Postgraduate School*, June 2000.
27. Dellicker, S., Benney, R., Patel, S., Williams, T., Hewgley, C., Yakimenko, O., Howard, R., and Kaminer, I., "Performance, Control and Simulation of the Affordable Guided Airdrop System", *AIAA Guidance, Navigation, and Control Conference*, Denver, CO, August 14-17, 2000.
28. Dobrokhodov, V, Yakimenko, O., and Junge, C., "Six-Degree-of-Freedom Model of a Controlled Circular Parachute", *AIAA Atmospheric Flight Mechanics Conference, Monterey, CA, August 5-8, 2002.*
29. Johnson, J., Yakimenko, O., Kaminer, I., and Dellicker, S., "On the Development and Pre-Flight testing of the Affordable Guided Airdrop System for G-12 cargo parachute," *Proceedings of 16th AIAA Aerodynamic Decelerator Systems Technology Conference and Seminar*, Boston, MA, May 21-24, 2001.
30. Yakimenko, O., Kaminer, I., and Dellicker, S., "Preliminary Design and Control Strategy Analysis of the Affordable Guided Airdrop System," *Proceedings of the 9th Mediterranean Conference on Control and Automation*, Dubrovnik, Croatia, June 27-29, 2001.
31. Precision Airdrop Technology Conference and Demonstration, http://yuma-notes1.army.mil/mtea/patcadreg.nsf, 2001.
32. Poyner, D., "The Parachute Manual", *Para Publishing*, Santa Barbara, CA, Vol.2, 4th edition, 1991.
33. Knacke, T.W., "Parachute Recovery Systems Design Manual," *Para Publishing*, Santa Barbara, CA, 1992.
34. Mosseev, Yu., "Fluid-Structure Interaction Simulation of the US Army G-12 Parachute," Report 17-01-RDD Ozon, Contract No. 68171-01-M-6342, http://www.mtu-net.ru/mosseev/rd.htm.
35. Benney, R., Brown, G., and Stein, K., "A New Pneumatic PMA: Its Use in Airdrop Applications," AIAA 99-1719, *15th CAES/AIAA Aerodynamic Decelerator Systems Technology Conference*, Toulouse, France, June 9-11, 1999.
36. Affordable Guided Airdrop System (AGAS) Valve System trade Study and Preliminary Design, *Vertigo, Inc.*, December 30, 2000.
37. AGAS III Prototype Testing Series 3: 23-27 July 2001, *Vertigo, Inc.*, August 1, 2001.
38. Kelly, K., and Pena, B., "Wind Study and GPS Dropsonde Applicability to Airdrop Testing," *Proceedings of 16th AIAA Aerodynamic Decelerator Systems Technology Conference and Seminar*, Boston, MA, May 21-24, 2001.
39. Hattis, P., Fill, T., Rubenstein, D., Wright, R., Benney, R., and LeMoine, D., "Status of an On-board PC-based Airdrop Planner Demonstration,"*16th AIAA Aerodynamic Decelerator Systems Technology Conference*, Boston, MA, May 21-24, 2001.
40. Pontrjagin, L., Boltjanskiy, V., Gamkrelidze, R., and Mishenko, E., "Mathematical Theory of Optimal Processes," *Nayka*, Moscow, 1969 (in Russian).
41. Drozd, V., *Irvin Aerospace Canada Ltd. - NPS* Correspondence, 2001.